Coupled geomechanics and flow simulation for time-lapse seismic modeling

Susan E. Minkoff*, C. Mike Stone‡, Steve Bryant**, and Malgorzata Peszynska§

ABSTRACT

To accurately predict production in compactible reservoirs, we must use coupled models of fluid flow and mechanical deformation. Staggered-in-time loose coupling of flow and deformation via a high-level numerical interface that repeatedly calls first flow and then mechanics allows us to leverage the decades of work put into individual flow and mechanics simulators while still capturing realistic coupled physics. These two processes are often naturally modeled using different time stepping schemes and different spatial grids—flow should only model the reservoir, whereas mechanics requires a grid that extends to the earth's surface for overburden loading and may extend further than the reservoir in the lateral directions. Although spatial and temporal variability between flow and mechanics can be difficult to accommodate with full coupling, it is easily handled via loose coupling. We cal- culate the total stress by adding pore pressures to the effective rock stress. In turn, changes in volume strain induce updates to porosity and permeability and, hence, dynamically alter the flow solution during simulation. Incorporating the resulting time-dependent pressures, saturations, and porosities (from coupled flow and mechanics) into Gassmann's equations results in seismic wave velocities and densities that can differ markedly from those calculated from flow alone. In a synthetic numerical experiment based on Belridge field, California, incorporation of coupled flow and mechanical deformation into time-lapse calculations produces compressional wave velocities that differ markedly from those produced by flow alone. In fact, it is the closing of the pores themselves (reduction in permeability) in this example which has the greatest impact on fluid pressures and saturations and, hence, elastic wave parameters such as velocity.

INTRODUCTION

Over the last decade, time-lapse seismic modeling has gained tremendous ground as a technology of interest to companies wishing to explore producing reservoirs for trapped oil and gas. The basic methodology involves imaging a section of the subsurface at periodic intervals and differencing these collected data sets to try to analyze the state of the field. As pointed out by Nur (1989), traditional production methods may miss 70–90% of the fluids in a field. Therefore, to increase oil and gas reserves, we must explore carefully selected enhanced recovery techniques. Time-lapse seismic imaging can highlight pockets of trapped oil and gas, but perhaps more significantly, it allows us to improve our overall understanding of the key reservoir parameters—porosity, permeability, saturation and temperature—which are used to assess the feasibility of different production scenarios.

Time-lapse seismic studies require careful collection and processing of the data [see Lumley et al. (1997) and Rickett and Lumley, (2001)]. In fact, interesting field studies are underway to assess the usability of data recovered from permanently deployed sensors [see, for example, papers by Beasley et al. (1997) and Ebrom et al. (1998)]. Numerical time-lapse studies carried out on computers can provide inexpensive but valuable information about the visibility of subsurface features in the face of inconsistencies in source and recording equipment, data acquisition geometry, and other types of noise.

One area in which time-lapse seismic analysis is just beginning to be used is in the modeling of compactible (or weak-formation) reservoirs. Despite the fact that these reservoirs

introduce a host of new data processing and modeling difficulties, such fields often have ideal characteristics for applying time-lapse analysis. As pointed out by Lumley et al. (1997), certain reservoir conditions act as indicators that time-lapse analysis is likely to be successful. These conditions include shallow reservoirs with low dry bulk modulus (high rock compressibility) and high porosity—exactly the conditions which are found in weak-formation fields. In one of the first papers to include both flow parameters and mechanical stress in time-lapse calculations, Olden et al. (2001) model a 2D gas-water reservoir using a flow simulator. They calculate changes to elastic rock properties from changes to pressure and saturation via fluid substitution and then condition the rock properties a second time (using empirical rock physics relationships derived from lab measurements) to incorporate stress changes. They indicate that their modeling could be improved by developing software that incorporates the different types of data in a more straightforward fashion. Pennington et al. (2001) describe a case study in which faulting in the reservoir gives unexpected time-lapse results. Xu and Nur (2001) integrate reservoir simulation and satellite imaging to detect subsidence and to continuously monitor hydrocarbon production. Their model is again 2D and assumes single-phase flow. Their aim is to better estimate reservoir permeability via continuous radar monitoring. Vidal et al. (2002) monitor an underground gas-storage reservoir. They use flow simulation to estimate pore pressures and saturations, and then geomechanical stresses are calculated from the pore pressures. Again, they use empirical rock physics models (Hertz-Mindlin theory) to modify seismic velocity based on stress changes. Finally, Guilbot and Smith (2002) develop a set of equations that allow them to calculate changes to overburden and reservoir velocities from compaction. They apply their method to data from the Ekofisk field in the North Sea.

In this paper, we describe a very different type of study. We have coupled together a 3D finite-element multiphase flow code with an equally complex 3D finite-element mechanical deformation code via a staggered-in-time algorithm. These two codes were chosen primarily because they model a variety of realistic production environments. The two simulators are loosely coupled via an interface which allows two-way passage of information between the simulators (pressures to mechanics, updated porosity and permeability to flow). In this way, we are able to leverage the substantial development effort which has gone into the two codes (Minkoff et al., 2003). Moreover, our algorithm serves as a prototype for coupling any two such independently-developed codes. Output pressures, saturations, and porosities from the coupled code are then fed directly into Gassmann's equations to calculate changes to elastic rock properties for seismic time-lapse analysis. Preliminary results from this project were described in the paper by Minkoff et al. (1999). In that work, the authors analyzed a synthetic experiment based on a single layer of Belridge field, California. Porosity changed dynamically during flow simulation as a result of stress effects. Permeability was held fixed. Time lapse analysis indicated that flow and mechanics coupled together can impact seismic properties.

In the remainder of this paper, we describe the reservoir flow simulator, the mechanical deformation code, the coupling algorithm, and the modifications made to the two simulators in order to link them together. We detail how time-lapse seismic modeling of compactible reservoirs differs from 4D analysis of fields in which the reservoir rock is assumed fixed. Finally we describe two realistic numerical experiments based on Belridge field. The first experiment is a complex multilayer example which closely models materials found in the extensive diatomite reservoir of Belridge field. For this numerical experiment, porosity changes dynamically due to stress effects. The second numerical experiment we describe focuses on a single layer of Belridge diatomite material, but both porosity and permeability change dynamically during coupled simulation. These numerical experiments clearly illustrate that seismic time-lapse rock properties determined from coupled flow and mechanical deformation modeling can differ markedly from those derived from flow alone.

DESCRIPTION OF SIMULATORS

Reservoir simulator

The fluid flow simulator, IPARS (Integrated Parallel Accurate Reservoir Simulator) (Parashar et al., 1997; Wang et al., 1997; Wheeler et al., 1999) built at the University of Texas, is a subsurface simulator which includes multiple physical flow models. The IPARS simulator was chosen for this work because of its versatility and sophistication. As an example, IPARS is uniquely able to follow geologic structure (especially faults) via blocking, making it a good choice for a complex flow and mechanics simulator. [For further details on the multiblock technique in IPARS, see Arbogast et al. (1996), Yotov (1998), Peszynska et al. (1999), Wheeler et al. (2000), Lu et al. (2001), and Peszynska et al. (2002).]

In this paper, we focus on one of the flow models in IPARS—the black oil model—which is the simplest model that includes all three fluid phases (oil, gas, and water) needed for seismic time-lapse studies (see Lumley, 1995). We make the assumption here that the reservoir is isothermal and that the permeability tensor is diagonal. Although fluid viscosity generally depends on pressure, in this paper we assume it is constant because it varies so little over the pressure range seen in our numerical experiments.

In this work, we use the default no-flow Neumann boundary conditions applied on the external boundary. Numerically, the black oil model code is fully implicit, 3D, and uses an expanded mixed finite-element method to maintain local conservation of mass (Lu, 2000; Lu et al., 2001).

Black oil formulation.—We assume that up to three phases and three components are present. The uppercase subscripts W, O, and G are used for the fluid components: water, heavy hydrocarbon or oil, and light hydrocarbon or gas, respectively. Lowercase subscripts w, o, and g are used for the fluid phases. The model is partially miscible. [For references to the black oil model, see Peaceman (1977) and Lake (1989)].

Given that N_I is the stock tank volume of component I per unit pore volume, ϕ is porosity, R_o is the stock tank volume of gas dissolved in a stock tank volume of oil, and q_I is the total stock tank rate of injection of component I, the mass balance equations are

$$\frac{\partial}{\partial t}(\phi N_G) = -\nabla \cdot (\mathbf{U}_g + R_o \mathbf{U}_o) + q_G,$$

$$\frac{\partial}{\partial t}(\phi N_I) = -\nabla \cdot \mathbf{U}_i + q_I \quad I = oil, water. \quad (1)$$

Darcy's Law gives the mass velocity $\mathbf{U}$ of phase i (here $i =$ oil, gas, or water) as

$$\mathbf{U}_i = -\frac{\mathbf{K}k_{ri}}{B_i\mu_i} \cdot (\nabla P_i - \rho_i g \nabla D). \qquad (2)$$

Here, $\mathbf{K}$ is the absolute permeability tensor, and k_{ri} is the relative permeability of phase i. B_i is the formation volume factor for phase i. P_i is pressure, μ_i is viscosity, and ρ_i is density. Gravity has magnitude g, and D is depth. Finally, the saturations must satisfy the constraint

$$S_g + S_o + S_w = 1, \qquad (3)$$

and capillary pressures are defined by

$$P_{cow}(S_w) = P_o - P_w, \quad P_{cgo}(S_g) = P_g - P_o. \qquad (4)$$

The gas component is soluble in the oil phase. The maximum concentration of gas that can be dissolved in the oil phase at a given pressure is given by R_s. Reducing the pressure of a volume of gas-saturated oil causes gas to come out of solution and form a free gas phase. Thus two-phase conditions and three-phase conditions may prevail simultaneously in different regions of the same reservoir.

To complete the formulation, we must specify the state equations. We denote the stock tank density of component I by ρ_{IS}. Then, the water, gas, and oil phase densities are given, respectively, by

$$\rho_w = \rho_{WS}/B_w,$$
$$\rho_g = \rho_{GS}/B_g,$$
$$\rho_o = (\rho_{OS} + R_o\rho_{GS})/B_o. \qquad (5)$$

Gas and oil phase saturations are defined by

$$S_g = B_g(N_G - R_s N_O),$$
$$S_o = B_o N_O, \qquad (6)$$

and the water phase saturation is defined by the following two equations:

$$S_w = B_w N_w, \quad S_w = 1 - S_o - S_g. \qquad (7)$$

Geomechanical deformation modeling

The geomechanics code from Sandia National Laboratories, JAS3D, is a 3D, quasi-static finite-element code. Like IPARS for fluid flow, JAS3D is a sophisticated mechanical deformation code which has several unique capabilities. Specifically, JAS3D can accurately model large deformations, sliding contact surfaces, and both elastic and inelastic material responses from a wide array of constitutive models (Arguello et al., 1998). The finite element technology which is used in JAS3D is based on iterative quasi-static solvers which allow problems with large numbers of unknowns to be efficiently solved. Two iterative techniques are currently used in JAS3D: a preconditioned conjugate gradient technique (Biffle, 1993) and an adaptive dynamic relaxation technique (Stone, 1997).

We consider the following field equation governing the deformation of a body occupying a volume V:

$$\partial\sigma_{ij}/\partial x_j + \rho b_i = 0 \text{ on } V. \qquad (8)$$

Equation (8) is the quasi-static equation of motion, where σ is the Cauchy stress tensor, $\mathbf{x}$ is the position vector, ρ is the mass per unit volume, and $\mathbf{b}$ is a specific body force vector. The solution to Equation (8) is sought subject to the kinematic and traction boundary conditions:

$$u_i(x, t) = U_i(x, t) \text{ on } S_U, \qquad (9)$$

$$\sigma_{ij}n_j = s_i(x, t) \text{ on } S_T, \qquad (10)$$

where S_U represents the portion of the boundary on which kinematic quantities are specified (i.e., displacements u_i), n_j is a unit normal vector, and S_T represents the portion of the boundary on which tractions are specified. The boundary of the body is given by the union of S_U and S_T.

MODIFICATIONS TO FLUID FLOW

Traditional flow simulators initialize porosity and permeability at the start of the computation and leave them essentially fixed throughout the simulation. To dynamically incorporate output from mechanics into flow during simulation, quantities involving porosity and permeability need to be updated each time the code completes a JAS3D step.

In traditional flow simulators, small changes to reservoir porosity ϕ are accounted for by the following linear expression:

$$\phi = \phi^*(1 + c_r(P - P^*)), \qquad (11)$$

where ϕ^* is the initial porosity at initial pressure P^*, P is current pore pressure, and the rock compressibility c_r is a constant (typically on the order of 10^{-7} to 10^{-10} Pa^{-1}). Such small values for c_r accurately model linear elastic deformation but are not able to accommodate more complex models (i.e., nonlinearity or inelasticity). In our coupled simulator, we do not rely on equation (11) to determine changes to porosity from deformation. Porosity values at the beginning of each set of simulation time steps are calculated for the flow simulator (IPARS) from mechanics (JAS3D), as depicted in Figure 1. We are able to take advantage of the range of complex constitutive relations describing different materials available in JAS3D. (The numerical experiments described in this paper use a plastic cap model, for instance.) The nonlinear system resulting from the finite-element discretization of equations (1) and (2) is solved via Newton's method. Porosity updates at time step $n + 1$ (from mechanics) are directly incorporated into the Newton method residual for the flow equations. Mass is conserved, and the Newton update accounts for a decrease in pore space (for example) by increasing the well rates and pressures at the next time step.

Nonetheless, initial numerical experiments indicate that the flow solver may have difficulty accommodating large jumps in reservoir parameters produced by infrequent calls to the mechanics code. (Recall that one of the advantages of loose coupling is that displacements, stresses, and strains need not be recalculated each time a flow step is taken as in full coupling.) We found that using an estimate of rock compressibility as a preconditioner to Newton's method helps the flow solver reach convergence after a return from the mechanics code. An approximate compressibility value is incorporated into the Jacobian calculation for the Newton system to guide the flow solver in the direction of porosity changes with pressure (Minkoff et al., 2003). In the second numerical experiment

described in this paper (single layer Belridge), we improve upon this idea. Equation (11), used in traditional flow simulators to update porosity, relates the current porosity to the change in fluid pressure from the initial state. In order to improve the computational performance of the flow simulator between geomechanics updates (explicit calls to JAS3D), we estimate small changes in porosity coming from pressure changes. We recast equation (11) into incremental form. The expression for porosity at time step n becomes

$$\phi^n = \phi^m (1 + c_r(P^n - P^m)), \qquad (12)$$

where the superscript m denotes porosity calculated from the most recent output of the mechanics code (JAS3D) at pressure P^m.

Dynamic updates to absolute permeability during flow simulation impact large portions of the code. The values of transmissibility are generally assumed fixed in uncoupled flow simulators. In our code, both the transmissibilities and the well model must be updated after each mechanics step to account for the permeability changes induced by strain. [For more detail on these modifications to the fluid flow code, see Minkoff et al. (2003)].

MODIFICATIONS TO MECHANICS

The mechanics code is capable of calculating point-wise changes in pore volume in the reservoir, coming (for example) from field production, pressure decrease, and then compaction. To calculate these field property changes in the coupled code, the reservoir simulator sends the pore pressure field to the geomechanics part of the code where it is used in the calculation of total stress:

$$\sigma_{ij}^T = \sigma_{ij} + p\delta_{ij}. \qquad (13)$$

Here, p the pore fluid pressure, δ_{ij} is the Kronecker delta function, and σ_{ij} is the "effective" stress which is used in the constitutive model. The total stress is used in the determination of the equilibrium state for the reservoir subject to the overburden loads, kinematic boundary conditions, and changing pore pressure field. On output, the geromechanics fcode provides an updated porosity ϕ at the current time step via the following expression:
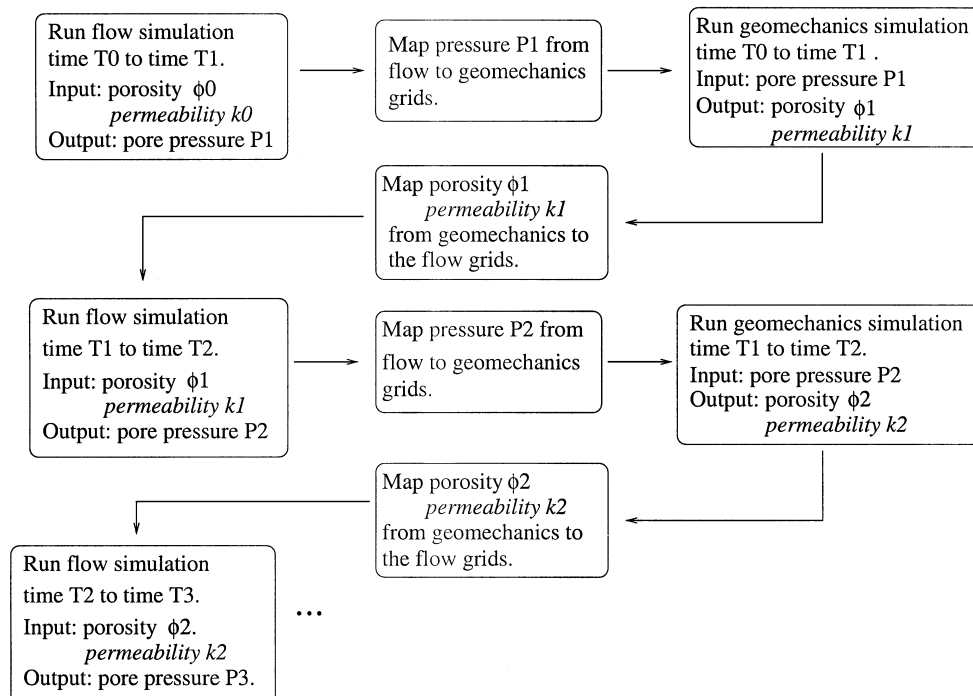
$$\phi = 1 - \frac{(1-\phi_0)}{e^{\epsilon_v}}, \qquad (14)$$

where ϕ_0 is the initial porosity, and ϵ_v is the total volume strain (the sum of the elastic and inelastic components of strain). We note that although JAS3D can handle thermal strains generated in the rock (temperature changes could be computed by the flow simulator and then passed to JAS3D in a similar fashion as the pore pressures), in this work we assume isothermal conditions.

For this work, we have chosen to use an exponential model relating permeability to volume strain (although any other functional form for permeability could be substituted into the code). This model was based on lab measurements made of permeability versus differential stress for several different rock types (A. Fossum, personal communication, 1999):

$$K = Ae^{B\epsilon_v}. \qquad (15)$$

Staggered Geomechanics/Reservoir Flow Simulation:

FIG. 1. Flow chart for loose coupling algorithm.

Here A and B are material constants and ϵ_v is again the total volume strain. This empirical relationship assumes permeability changes will be isotropic.

THE LOOSE COUPLING ALGORITHM

Various algorithms have been investigated for coupling together two or more distinct physical simulators. These algorithms range from the tightest coupling of physics (full coupling) to the weakest (one-way coupling). In this work, we wish to model realistic physics while making use of the two sophisticated simulators described earlier in this paper (IPARS and JAS3D). Our algorithm passes information between the two simulators via a high-level interface. Related two-way loose coupling algorithms have been investigated by Fung et al (1994) Settari and Mourits (1994), and Settari and Walters (1999).

In our algorithm, the user designates a mechanics time step and a separate flow time step. (We will call the time interval between mechanics time steps Δt, where $\Delta t_1 = t_1 - t_0$; a typical value of Δt being anywhere from one month to one or two years.) The flow simulator runs first and will likely break the Δt_1 time interval into multiple flow time steps (typically on the order of a fraction of a day to a few days). At the end of the time interval Δt_1, the pore pressure is passed to the mechanics code, and the mechanics code then runs the simulation for that same (prior) Δt_1 time interval. The geomechanics code may take only one time step for this time interval (or at least it will likely take different subtime steps relative to the flow simulator time step sequence). The mechanics calculation is quasi-static, nonlinear, and time independent. In these calculations, we have no time-dependent material response such as creep. However, there may be a time lag in subsidence relative to production changes due to the flow properties of the rock. For example, we might stop production of the well, but subsidence might continue to occur as reservoir pressure gradients equilibrate with the overburden.

The mechanics code uses the pore pressures to calculate strains and ultimately updates to porosity and permeability. Using the updated values of the flow parameters from mechanics, the coupled code then simulates flow for the next time interval $\Delta t_2 = t_2 - t_1$. The two-way staggered-in-time coupling algorithm proceeds until the both simulators reach the final time t_{end}. The loose-coupling algorithm is shown as a flow chart in Figure 1.

Between the flow and mechanics simulations in Figure 1 lies a column devoted to mapping output and input quantities from one simulator to the other. This column is necessary because the loose coupling algorithm does not require the two simulators to use the same computational grid. (In fact, this is an advantage of loose coupling!) The flow domain is typically a subset of the mechanics domain. The flow simulator will only model the reservoir, whereas the mechanics code may need to extend further in the lateral directions than the reservoir, will surely need to extend up to the earth's surface (for overburden loading), and may cover an area below the reservoir as well. Note that fully coupled simulators typically assume a single computational domain requiring unnecessary calculations on the reservoir side. The current algorithm also does not require the two codes to have the same grid spacing in the parts of the domain where there is overlap (the reservoir). Physically, there may be a sound reson why the spatial discretization on the flow side will differ from that for mechanics (examples: multiple material layers in the reservoir or a need for finer resolution to capture complex physics). We have chosen here to use a software package from Sandia's engineering suite, MAPVAR (Wellman, 1999) for the upscaling. Different spatial domains for flow and mechanics are sent to MAPVAR, and variables are mapped on the overlapping portions of these domains. MAPVAR uses either nodal averaging, constrained least squares, or direct transfer for data interpolation. In this work, we are using constrained least squares, which is the most accurate of the three options because it is able to capture gradients in the solution. The interpolation within MAPVAR can be done on either undeformed or deformed geometries. Computation time for the data transfer is insignificant compared to the computation times for the flow and geomechanics codes.

TIME-LAPSE SEISMIC MODELING

Time-lapse seismic modeling fundamentally relies on being able to incorporate reservoir (fluid flow) effects into elastic wave propagation. We use Gassmann's equations to convert the time-dependent reservoir pressures and saturations resulting from the flow simulation (or flow simulation and geomechanics) into elastic rock parameter changes (Gassmann, 1951). Gassmann's equations provide a way to compute the effective bulk and shear moduli (K and μ, respectively) of reservoir rock saturated with a given composition of pore fluids from the elastic moduli of the dry rock. These equations are

$$\mu_{sat} = \mu_{dry}, \tag{16}$$

$$\frac{K_{sat}}{K_{solid} - K_{sat}} = \frac{K_{dry}}{K_{solid} - K_{dry}} + \frac{K_{fluid}}{\phi(K_{solid} - K_{fluid})}. \tag{17}$$

Gassmann's equations require knowledge of (1) the effective bulk modulus of the pore fluid K_{fluid}, (2) the porosity ϕ, (3) the bulk and shear moduli of the dry rock with empty pores K_{dry}, μ_{dry}, and (4) the bulk modulus of the mineral material making up the rock K_{solid}.

In the examples described in this paper, we assume a fixed oil and water phase bulk modulus but used a modified ideal gas law to calculate the gas modulus [see Dake (1978), Lumley (1995)]. The modified ideal gas law includes a "Z factor" to correct for the difference between reservoir and atmospheric pressures. The total fluid bulk modulus is then calculated as

$$\frac{1}{K_{fluid}} = \frac{S_w}{K_w} + \frac{S_o}{K_o} + \frac{S_g}{K_g}. \tag{18}$$

The dry moduli are determined entirely by rock physics measurements made on core samples at differing differential pressures (where differential pressure is the difference between overburden and pore pressures). To calculate the total fluid density, we calculate the individual phase densities via equation (5) and then take a saturation-weighted average of the three phase densities as follows:

$$\rho_{fluid} = S_w \rho_w + S_o \rho_o + S_g \rho_g. \tag{19}$$

Finally, from Gassmann's equations and relationships between elastic parameters, we can determine the density ρ, compressional wave velocity V_p, and shear wave velocity V_s at a given fluid saturation, pressure, and porosity:

$$\rho_{sat} = (1 - \phi)\rho_{solid} + \phi\rho_{fluid}, \tag{20}$$

$$Vp_{sat} = \sqrt{\frac{K_{sat} + \frac{4}{3}\mu_{sat}}{\rho_{sat}}}, \tag{21}$$

$$Vs_{sat} = \sqrt{\frac{\mu_{sat}}{\rho_{sat}}}. \tag{22}$$

There are a number of places where output from coupled flow and mechanics used as input to Gassmann's equations will strongly influence the results. When pore fluid pressures are used as input loads for the mechanics calculation, new values of reservoir porosity and permeability resulting from stress changes in turn affect future pressure and saturation calculations from flow. Items (1) and (3) above (K_{fluid} and K_{dry}, μ_{dry}) are affected by pressure changes [as is item (2) porosity indirectly via geomechanics]. The fluid modulus is also affected by saturations. Porosity [item (2)] is directly updated in the deformation code and will, therefore, also differ from flow simulation alone. In fact, one traditionally assumes porosity is constant when applying Gassmann's equations. In our case, porosity will change (dramatically in places) with time. The level of impact coupled simulation can have on seismic properties is illustrated in the Belridge field examples described below.

NUMERICAL EXAMPLES

The examples we describe here are based on data from Belridge field. Belridge is located west of Bakersfield, California, and was the fifth most productive field in the U.S. in 1996. In fact, the field was estimated to have more than 5×10^8 m^3 of original oil-in-place. The field contains two reservoirs: a small reservoir located in the shallow Tulare sand, and a slightly deeper reservoir located in diatomite, which extends nearly 305 m in depth. Despite the fact that this large diatomite reservoir was discovered in the early 1900s, by the mid 1990s, most of the production was still focused on the Tulare reservoir (Fredrich et al., 1996). The diatomite has unusual geologic properties which make production difficult. This reservoir has a large pore space (porosities range from 45% to 70%), but very low permeability ($\sim$0.1 md). In the mid 1970s, hydraulic fracturing (and hence the introduction of new flow paths) allowed production in this field for the first time. However, with increased production came substantial subsidence (up to 6 m at the earth's surface) and hence well failures, which by the mid 1990s amounted to a well failure rate of 2–5% annually (Fredrich et al., 1996).

Minkoff et al. (1999) describe a synthetic experiment based on Belridge field which focuses on a single layer of diatomite material (layer J). In that paper, porosity was modified dynamically during flow simulation, but permeability remained fixed. In this paper, we describe two related numerical experiments. The first is a more complete Belridge simulation in which we model all 18 material layers (in depth) which describe the actual reservoir. Again, we assume permeability does not change during simulation but modify porosity based on the output of

the mechanical stress calculation. The second example is a single layer problem focused on the weakest layer of diatomite (layer J). The computational domains for mechanics and flow used in the multilayer numerical experiment and the relative position of layer J in the overall reservoir are shown in Figure 2. In the single layer synthetic experiment presented in this paper, both permeability and porosity change substantially during flow simulation as a result of mechanical compaction. We note that diatomite is an unusual material with a very large pore space that dramatically deforms due to changes in pressure and fluid saturation. While we do not claim that studies done on diatomite produce typical oil field behavior, we do feel the numerical experiments illustrate the capabilities of the coupled code for fields in which large displacements occur.

Multilayer Belridge experiment

The first example we describe closely follows the geologic structure of Belridge field in depth and field properties. The reservoir is assumed to be rectangular with four production wells in the corners of the domain. Each well extends to a slightly different depth in the reservoir. The computational domain corresponds to a single section of the total reservoir (in the horizontal directions), and hence is unusual because it extends noticeably further in z than in x and y. The reservoir domain is broken into 21 grid blocks in x and in y, and 22 blocks in z. Grid spacing is fixed at 5.03 m in each of the lateral directions, but varies in z. The top of the reservoir (located at a depth of 210 m from the surface) has an initial pore pressure of 2.28 MPa. Initial water saturation is 31.4% with minimal free gas of 5%. Porosity is initially uniform throughout the domain at 50%, and permeability is heterogeneous and anisotropic with values ranging from 0.002 to 0.1385 md. Permeability (based on field measurements) is consistently ten times greater in the horizontal directions than in depth. We simulate 10 years of coupled
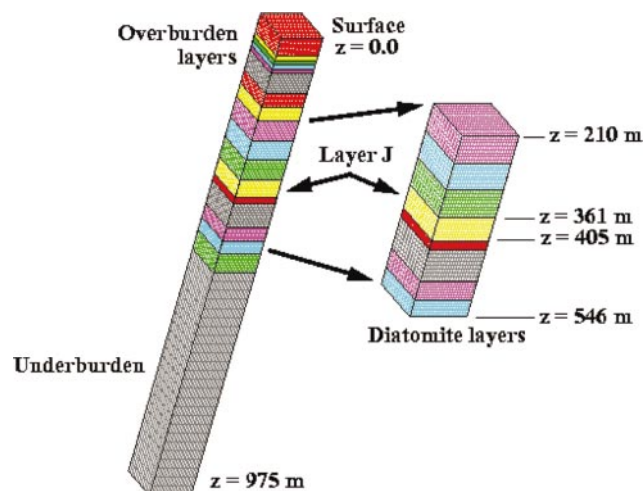

FIG. 2. Simulation domains for the multilayer Belridge field synthetic experiment. Leftmost figure is the computational domain for mechanical deformation. The figure on the right is the computational domain for reservoir simulation. Numerical experiment 2 focuses on layer J, which is labeled in the figure as well.

flow and mechanics. IPARS takes time steps of 0.2 to 10 days, and the JAS3D time steps occur every 30 days.

JAS3D contains more than 50 different constitutive relationships which can be used to simulate deformation of a range of materials. We use a modified Sandler-Rubin cap-plasticity constitutive relationship (Sandler and Rubin, 1979) developed specifically to model compaction of Belridge diatomite (Fossum and Fredrich, 2000). It provides a more realistic representation of the mechanical behavior of porous soil or rock than the basic Drucker-Prager model (Drucker and Prager, 1952) by incorporating lode-angle dependence of yield in the deviatoric plane and nonassociativity in the meridional plane on the shear failure surface. The loading function is assumed to be isotropic and to consist of two parts: an ultimate shear failure surface which serves to limit the maximum shear stresses attainable by the material, and an elliptically shaped strain-hardening surface, or "cap," that produces plastic volume and shear strains as it moves. This model is described more thoroughly in papers by Fossum et al. (1995), Arguello et al. (1998), and Minkoff et al. (2003). In both the examples described in this paper which involve diatomite, the vertical sides of the model are constrained from movement normal to the boundary. The prescribed in-situ stress state at the initial time is due to gravity loading and calculated from the density of the overlying materials. The horizontal principal stresses (x and y) were calculated by multiplying the vertical principal stress (z) by factors of 0.65 and 1.20, respectively (Fredrich et al., 2000).

In the first numerical example, the JAS3D model contains 18 different material layers corresponding to 12 different sets of material properties. Layer depths and material moduli used for the geomechanics calculation are given in Table 1. Only the diatomite reservoir is included in the flow grid. The mechanics grid extends outside the reservoir and includes the overlying air sands and Tulare reservoir and underlying porcellanite. In fact, the flow domain was discretized into 9702 total grid blocks. In contrast, there were 37 548 total grid blocks used for the mechanics calculation. All diatomite materials are modeled using the cap-plasticity constitutive model. The more standard Drucker-Prager constitutive relationship is used for modeling stress and strain in the remaining materials.

In this example, the deformation portion of the coupled code produces dynamic changes to porosity, but permeability is held fixed. At the start of simulation, the pore pressure decreases due to production are fairly uniform throughout the field (see

Table 1. Material layer properties used in Belridge experiment 1 for mechanical deformation calculation.

Type of material	Layer depth (m)	Young's modulus (MPa)	In reservoir grid?
Air sands	46	124	no
Upper Tulare	91	241	no
Lower Tulare	210	241	no
Diatomite layer G	261	329	yes
Diatomite layer H	311	434	yes
Diatomite layer I	361	546	yes
Diatomite layer J	404	414	yes
Diatomite layer K	421	494	yes
Diatomite layer L	479	775	yes
Diatomite layer M	514	1121	yes
Diatomite layer N	690	1121	yes
Porcellanite	1158	469	no

Figure 3). But by year 7, most of the change in pore pressure has accumulated in layer J, the portion of the reservoir which undergoes the majority of compaction (see Figure 4). Layer J is the weakest of the diatomite layers, with an elastic modulus that is 15 times weaker than sandstone (Fredrich et al., 2000; J. Fredrich, personal communication, 1999). One can clearly see in Figure 5 that by year 7, porosity has dropped from its initial value of 50% down to 48.5% in layer J. The pore volume decrease is calculated from the change in strain as shown in Figure 6. Vertical displacement is approximately 3 m at the earth's surface by year 7. The displacement profile is shown in Figure 7. The low permeability of the reservoir rocks and
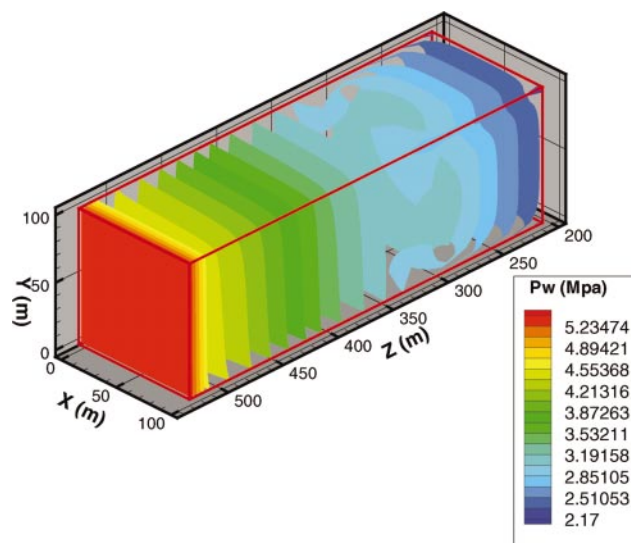

FIG. 3. Pore pressure contours (in MPa) for the multilayer Belridge field numerical experiment after one year of coupled flow and mechanical deformation modeling. Axis units shown are in meters.
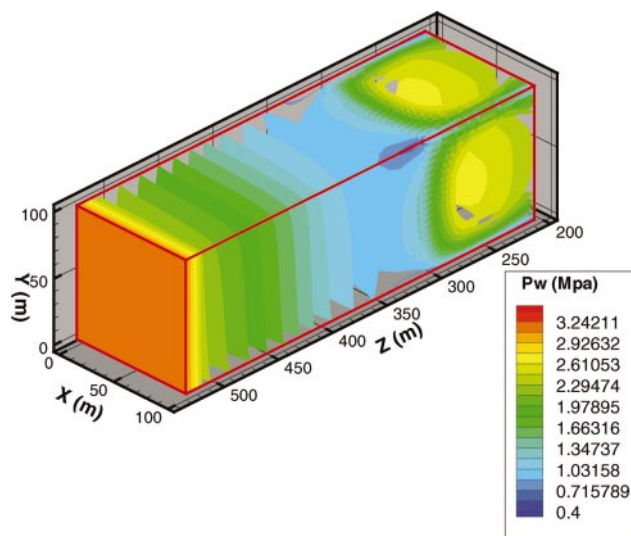

FIG. 4. Pore pressure contours (in MPa) in the multilayer Belridge field reservoir after seven years of coupled flow and mechanical deformation modeling. Axes are in meters.

heavy oil in this field make movement of fluids to the wells difficult. However, to conserve mass while simulating flow in a compacting reservoir, the fluids must move out the wells. This phenomenon explains the large decrease in pore pressure seen in layer J (Figure 4).

In order to determine seismic rock property changes in the simulated reservoir with time, we need the moduli of the solid diatomite rock as well as rock physics curves which correlate changes in modulus to pressure. For the solid matrix diatomite, we used modulus values for opal (Birch, 1966), namely that K_{solid} is 15 457 MPa and μ_{solid} is 18 000 MPa. The solid rock density ρ_{solid} was taken to be 2.25 g/cm^3. Pressure dependent dry rock values were taken from clean diatomite measurements of the Lost Hills formation. These values were provided to us
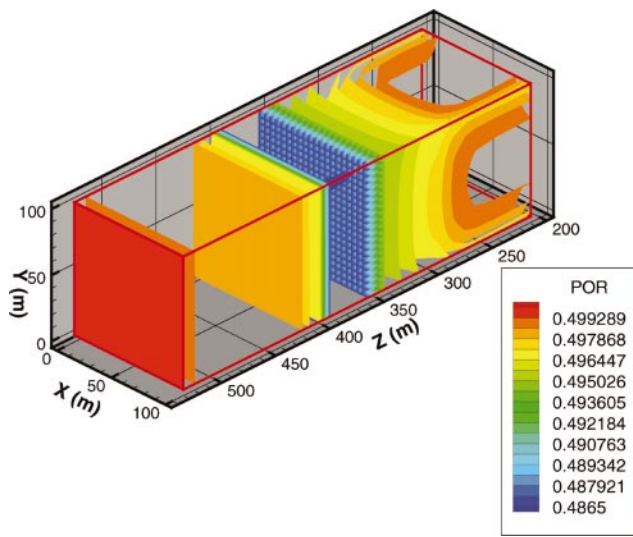

FIG. 5. Porosity (dimensionless) after seven years of coupled flow and mechanical deformation modeling for multilayer Belridge field numerical experiment. Axes are in meters.

by Joanne Fredrich of Sandia National Labs (personal communication, 1999) and are shown in Table 2. Figure 8 shows the time-lapse difference between the start of simulation and time 5 years for the saturated rock density calculated from flow alone and from coupled flow and mechanics. In the coupled simulation, changes to the density in layer J due to compaction are evident. The change in layer density is not evident from the time-lapse calculation based on flow alone. While the seismic velocities calculated via fluid substitution for this example showed some time lapse effects, they are not as striking as the changes in density.

Single-layer Belridge experiment

The second numerical example we describe is a synthetic experiment in which we model only layer J of the diatomite reservoir (see Figure 2). Like the multilayer Belridge example described above, this example has four production wells in the corners of the rectangular domain. The single-layer reservoir extends 44 m in depth. For flow simulation, the grid block spacing and number of points is the same in x and y as in the multilayer case. However, we now use 18 blocks in z, each of

Table 2. Diatomite modulus values used in rock physics analysis for the first numerical experiment (multilayer Belridge synthetic example). Lost Hills data courtesy of J. Fredrich, Sandia National Labs.

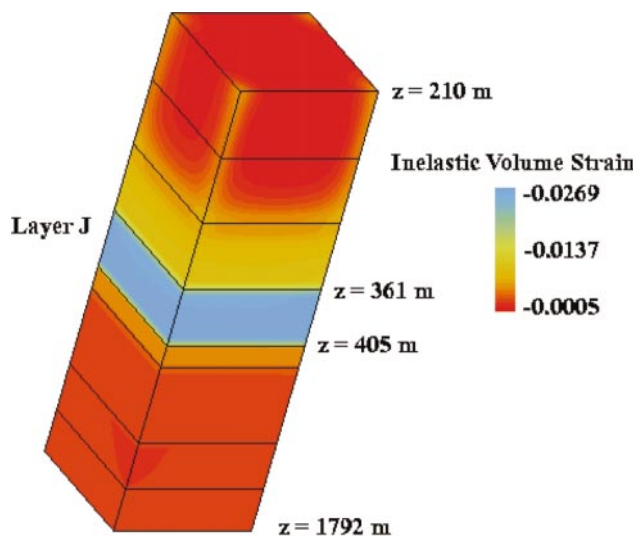|	Pressure (MPa)	Modulus (MPa)
Young's modulus	1.4	523
	6.9	1060
Shear modulus	1.4	217
	6.9	374

FIG. 6. Inelastic strain (dimensionless) after seven years of flow/mechanics simulation for the multilayer Belridge field numerical experiment.
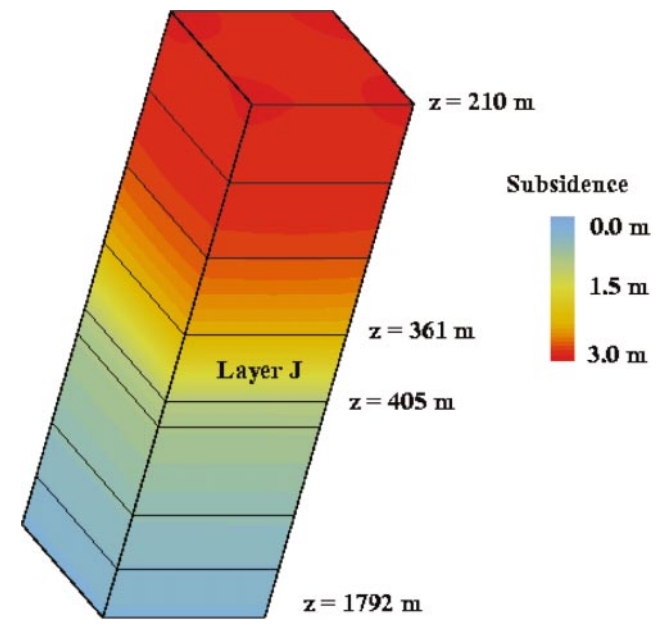

FIG. 7. Vertical displacement (in meters) after seven years of coupled simulation for the multilayer Belridge field numerical experiment.

width 2.4 m (a finer spacing than for the multilayer case). In this numerical experiment, the mechanics grid contains only one material and extends from the reservoir up to the earth's surface for overburden loading. The top of the reservoir is located at a depth of 361 m, and the corresponding initial pore pressure is 3.76 MPa. Initial fluid saturations are the same as in the multilayer case, and initial porosity is again taken to be uniform throughout the domain at 50%. However, for this numerical experiment we assume the permeability is isotropic and homogeneous everywhere at 0.1 md at the start of simulation. The calculation simulated five years of reservoir production with IPARS time steps ranging from 0.5 days to over 100 days, and calls to JAS3D performed initially every five days and gradually increasing to once a year. While adaptive time stepping was not used for the numerical experiments described in this paper, we have recently tested a local error adaptive time-step algorithm (Gear, 1971) to help optimize the number of calls to mechanics for the loose coupling algorithm. We believe computational savings over full coupling will be substantial. [For a comparison of coupling methods, see Dean et al. (2003).]

Besides the obvious difference in the simulation domain, this problem differs from the previous multilayer case in that both porosity and permeability change dynamically during simulation. As described in the section on modifications to fluid flow, large reservoir property changes produced by the mechanics code can place a burden on the flow solver. To ensure improved convergence for flow, we estimate porosity changes from incremental rock compressibility at flow time steps intermediate to explicit calls to JAS3D [explicit calls to JAS3D are shown in the flow chart,(Figure 1, right column)].

We contrast the results of flow simulation (IPARS) alone on this data with coupled flow simulation and mechanical de-

formation (IPARS/JAS3D). At the end of the five-year flow simulation the pressures had decreased by 40% from their initial values. At the end of the coupled flow and mechanics simulation, the pressures had decreased by 50%. A maximum difference in pressure between the two simulations occurs at the production wells (about 0.69 MPa).

The total strain at the end of the run is 2.5%. Figure 9 shows von Mises stress for the coupled simulation, and one can see 3D variations in stress at the wells due to different well schedules and different well completion depths. After five years of coupled simulation, a maximum subsidence of 0.41 m is calculated at the surface in the region of the wells. During coupled simulation, porosity decreases by 4%, but the permeabilities show the biggest change, decreasing from 0.1 to 0.001 md at the wells (see Figure 10 for the final permeability at the end of the coupled run).

For the time-lapse calculations, we used the rock physics data shown in Table 3 (courtesy of Z. Wang, ChevronTexaco, personal communication, 2003). The bulk and shear moduli were not directly measured but were backed out from other measured material properties. As shown in Tables 2 and 3, modulus values for diatomite can vary substantially from one location to another.
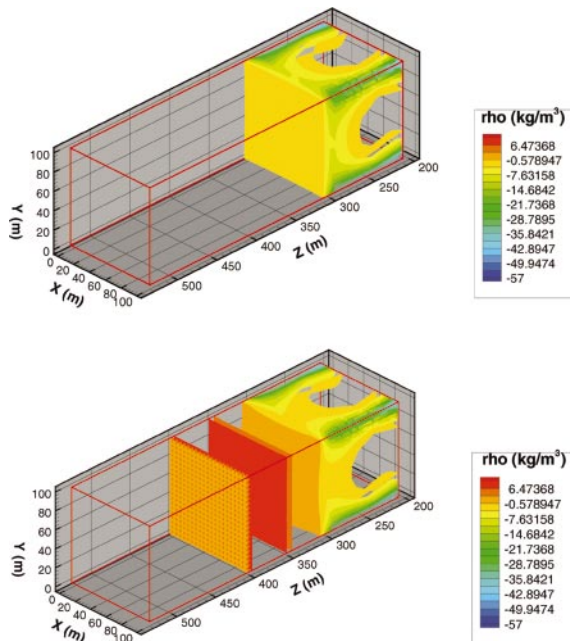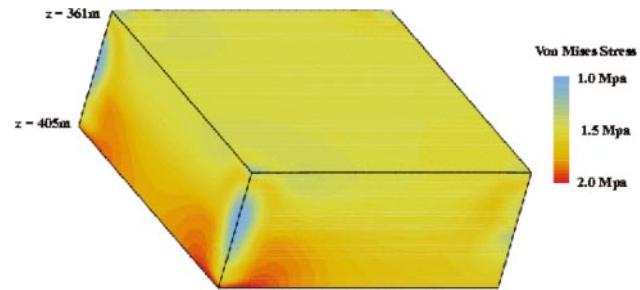

FIG. 9. Von Mises stress (in MPa) for the single-layer Belridge field numerical experiment at the end of five years of coupled flow and mechanical deformation modeling.

FIG. 8. Time-lapse change in saturated rock density (in kg/m^3) between start and end of five years of simulation for the multilayer Belridge field numerical experiment. Top figure shows density calculated from flow simulation alone. Bottom figure corresponds to density changes calculated from coupled flow and mechanics. Axes are in meters.
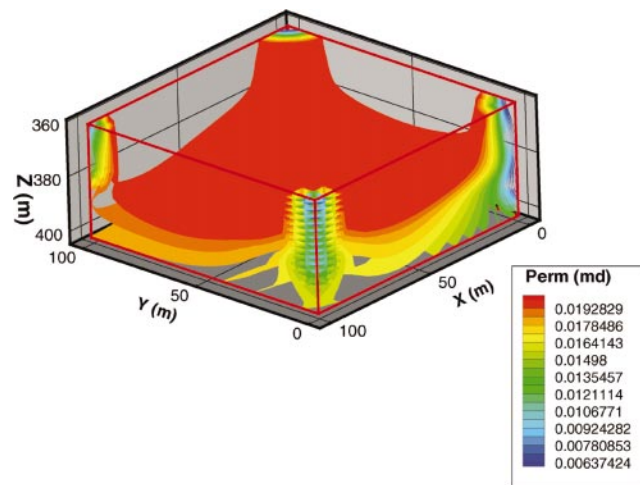

FIG. 10. Permeability (in md) at the end of five years of coupled flow and mechanical deformation modeling of the single-layer Belridge field data. At the start of simulation, the permeabilities are 0.1 md uniformly throughout the reservoir.

Table 3. Diatomite modulus values used in rock physics analysis for second numerical experiment (single layer Belridge synthetic example). Lost Hills data courtesy of Z. Wang, Chevron Texaco.

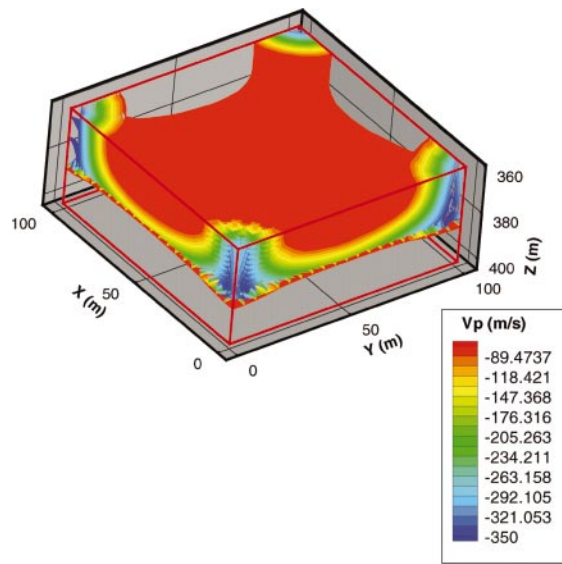|	Pressure (MPa)	Modulus (MPa)
Bulk modulus	1.9	1580
	6.2	1070
Shear modulus	1.9	1330
	6.2	1270

FIG. 11. Time-lapse calculation of the difference in saturated rock compressional wave velocity (in m/s) between the start and end of five years of coupled flow and mechanical deformation modeling for single-layer Belridge data.

In the first five years of coupled simulation, compressional wave velocity at the wells was reduced by 350 m/s, primarily due to gas coming out of solution (see Figure 11). Because the pore space is so large for the Belridge Field, seismic velocities tend to be very low. So this time-lapse velocity decrease is substantial. Figure 12 lists the inputs, outputs, and typical parameter units for fluid flow, mechanical deformation, and seismic modeling. We were surprised to find that the reduction in permeability had such a noticeable impact on the compressional wave velocities of the saturated reservoir rocks. Note that 1 darcy is equivilent to approximately 1×10^{-12} m^2 with typical seismic wavelengths being on the order of a few kilometers/second. Yet when we compared three numerical experiments (flow alone, flow and mechanics where only porosity changes during simulation, and coupled flow and mechanics where both porosity and permeability change during simulation), it was the third numerical experiment which showed the only substantial change in seismic wave velocity. Figure 13 shows the difference in compressional wave velocity computed at the end of simulation contrasted for these numerical experiments. The permeability change causes a seismic wave velocity discrepancy that would be detectable in a real field experiment.

We emphasize again that diatomite is an unusual material (with a pore space of 45–70% in places). For these synthetic numerical experiments, we assumed an initial porosity of 50%. Therefore, 50% of the time waves are traveling through fluids rather than rock. Sensitivity analyses show that some of the most striking changes we see in these numerical examples are due to changes in fluid modulus, not movement from one pressure point to another on rock moduli curves. Whether one uses the rock physics data in Table 2 or Table 3, the magnitude of change in V_p is essentially the same due to the significant variation in fluid saturation in this field with time. Coupling flow to mechanics can have a tremendous influence on reservoir properties and hence on output pressures and saturations.
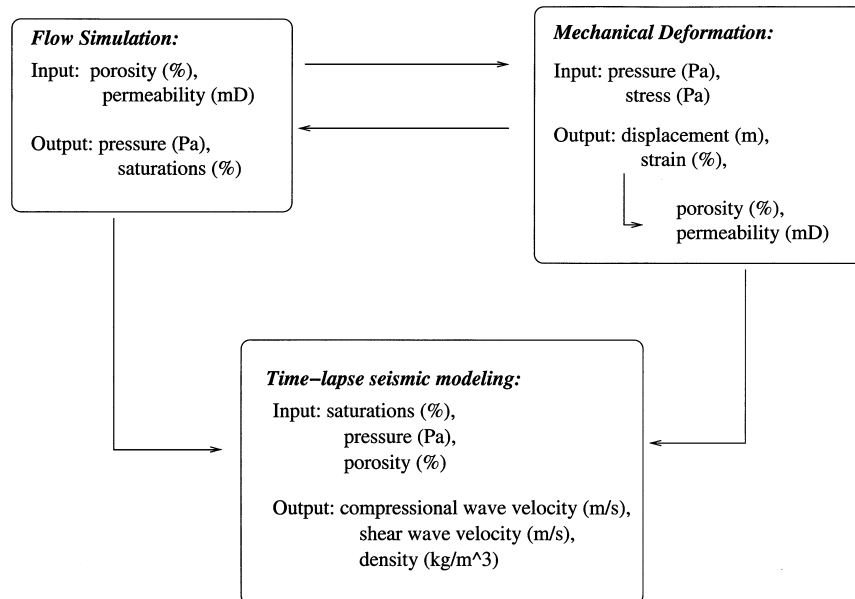

FIG. 12. Input and output parameters for three types of physics discussed in this work: fluid flow, mechanical deformation, and elastic wave propagation.
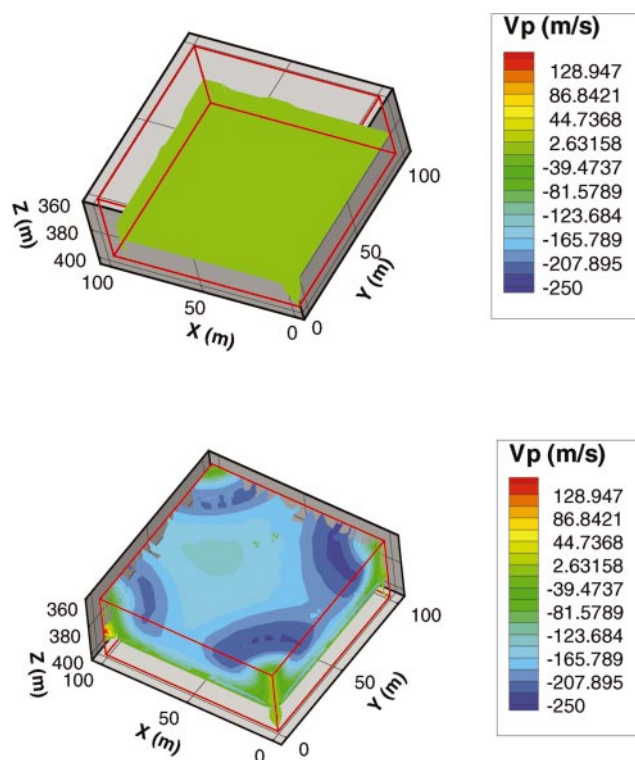
FIG. 13. (Top) Difference in compressional wave velocity (in m/s) between flow simulation alone and coupled flow and mechanical deformation modeling with only porosity changing dynamically. (Bottom) Difference in compressional wave velocity (in m/s) between flow simulation alone and coupled flow and mechanical deformation modeling with both porosity and permeability changing dynamically during simulation. Both figures correspond to single-layer Belridge numerical experiments at five years.

Pressures and saturations coming from coupled flow and mechanical deformation in turn affect seismic properties.

CONCLUSIONS

In this paper, we have described results of loosely coupling together two advanced 3D finite element simulators: IPARS from the University of Texas at Austin for flow and JAS3D from Sandia National Labs for mechanics. A high-level interface calls first the reservoir simulator for a fixed set of time steps and then the deformation code for that same (prior) set of time steps. Pore pressures from flow are used in the total stress calculation to determine mechanical property changes. The mechanics code then outputs updated flow parameters (porosity and permeability) for the next set of time steps. The loose-coupling algorithm is, therefore, staggered in time and includes two-way passage of information. Mass is conserved despite updates to porosity during flow by forcing fluids out the wells. The two simulators can take different time steps and have different spatial grids both inside and outside the reservoir interval.

When this coupled flow and mechanics simulator is used as input to a fluid substitution calculation, we can more accurately model reservoir changes in compactible fields. In our time-lapse analyses, porosity values used in Gassmann's equations are no longer fixed in time. Pressure and saturation-dependent

fluid and dry rock moduli are also affected by the stress changes incorporated into flow.

We have described two synthetic numerical examples based on data from the Belridge field diatomite reservoir. The first is a full-scale simulation (in depth) with 18 layers and 12 different materials. The diatomite reservoir is modeled using a modified Sandler-Rubin cap-plasticity constitutive model for nonrecoverable deformation. In this example, porosity changes, but permeability is held fixed. Strain accumulates in the weakest layer of the diatomite (layer J) causing 3–4 m of compaction at the surface. A pore pressure gradient gradually localizes in this weak layer as well. A fluid substitution calculation using the coupled data is able to identify the change in saturated rock density in the reservoir at layer J. By contrast, fluid substitution performed using flow simulation alone does not pick up this change in rock density.

The second example includes only the weakest diatomite layer of the reservoir. However, both porosity and permeability change dynamically due to stress. Permeability shows the biggest change, dropping two orders of magnitude during the five-year simulation. Seismic velocities are directly affected by these flow property changes. In fact, permeability changes are shown to greatly impact compressional wave velocity despite the vast difference in scale between these two rock properties.

We see little sensitivity in saturated rock parameters due to the size of the mechanics time steps taken, indicating that loose coupling is ideal for time-lapse seismic modeling of weak-formation reservoirs. In the future, we intend to incorporate adaptive time stepping based on the relative magnitude of displacement changes occurring in the reservoir. We also hope to validate our time-lapse calculations against well logs for real data examples.

REFERENCES

Arbogast, T., Wheeler, M., and Yotov, I., 1996, Logically rectangular mixed methods for flow in heterogeneous domains *in* Aldama, A., Aparicio, J., Brebbia, C. A., Gray, W. G., Herrera, I., and Pinder, G. F., Eds., Computational methods in water resources XI: Computational Mechanics Publications, 621–628.

Arguello, J., Stone, C., and Fossum, A., 1998, Progress on the development of a three-dimensional capability for simulating large-scale complex geologic processes: 3rd North American Rock Mechanics Symposium, Proceedings, Paper USA-327-3.

Beasley, C. J., Chambers, R. E., Workman, R. L., Craft, K. L., and Meister, L. J., 1997, Repeatability of 3-D ocean-bottom cable seismic surveys: The Leading Edge, **16**, 1281–1285.

Biffle, J., 1993, JAC3D—A three-dimensional finite element computer program for the nonlinear quasistatic response of solids with the conjugate gradient method: Sandia National Labs Technical Report SAND87-1305.

Birch, F., 1966, Compressibility; elastic constants, *in* Clark, S. P., Ed., Handbook of physical constants: Geological Society of America, 97–173.

Dake, L., 1978, Fundamentals of reservoir engineering: Elsevier Scientific Publishing Company.

Dean, R., Gai, X., Stone, C., and Minkoff, S., 2003, A comparison of techniques for coupling porous flow and geomechanics: Proceedings of the 17th SPE Reservoir Simulation Symposium, SPE 79709.

Drucker, D., and Prager, W., 1952, Soil mechanics and plastic analysis or limit design: Quarterly of Applied Mathematics, **10**, 157–164.

Ebrom, D., Krail, P., Ridyard, D., and Scott, L., 1998, 4-C/4-D at Teal South: The Leading Edge, **17**, 1450–1453.

Fossum, A., and Fredrich, J., 2000, Constitutive models for the Etchegoin sands, Belridge diatomite, and overburden formations at the Lost Hills Oil field, California: Sandia National Labs, Technical Report SAND2000-0827.

Fossum, A., Senseny, P., Pfeifle, T., and Mellegard, K., 1995, Experimental determination of probability distributions for parameters of a salem limestone cap plasticity model: Mechanics of Materials, **21**, 119–137.

Fredrich, J., Arguello, J., Deitrick, G., and de Rouffignac, E., 2000, Geomechanical modeling of reservoir compaction, surface subsidence, and casing damage at the Belridge diatomite field: SPE Reservoir Evaluation & Engineering, **3**, 348–359.

Fredrich, J., Arguello, J., Thorne, B., Wawersik, W., Deitrick, G., de Rouffignac, E., Myer, L., and Bruno, M., 1996, Three-dimensional geomechanical simulation of reservoir compaction and implications for well failures in the Belridge diatomite: Annual Technical Conference, Society of Petrolum Engineers, Expanded Abstracts, 195–210.

Fung, L.-K., Buchanan, L., and Wan, R. G., 1994, Coupled geomechanical-thermal simulation for deforming heavy-oil reservoirs: Journal of Canadian Petroleum Technology, **33**, 22–28.

Gassmann, F., 1951, Elastic waves through a packing of spheres: Geophysics, **16**, 673–685.

Gear, C., 1971, Numerical initial value problems in ordinary differential equations: Prentice-Hall.

Guilbot, J., and Smith, B., 2002, 4-D constrained depth conversion for reservoir compaction estimation: Application to Ekofisk field: The Leading Edge, **21**, 302–308.

Lake, L. W., 1989, Enhanced oil recovery: Prentice Hall.

Lu, Q., Peszynska, M., and Wheeler, M. F., 2001, A parallel multi-block black-oil model in multi-model implementation.: Proceedings of the 16th SPE Reservoir Simulation Symposium, SPE 66359.

Lu, Q., 2000, A parallel multi-block/multi-physics approach for multiphase flow in porous media: Ph.D. diss., University of Texas at Austin.

Lumley, D., 1995, Seismic time-lapse monitoring of subsurface fluid flow: Ph.D. diss., Stanford University.

Lumley, D. E., Behrens, R. A., and Wang, Z., 1997, Assessing the technical risk of a 4-D seismic project: The Leading Edge, **16**, 1287–1291.

Minkoff, S., Stone, C., Arguello, J., Bryant, S., Eaton, J., Peszynska, M., and Wheeler, M., 1999, Coupled geomechanics and flow simulation for time-lapse seismic modeling: 69th Annual International Meeting, Society of Exploration Geophysicists, Expanded Abstracts, 1667–1670.

Minkoff, S., Stone, C., Bryant, S., Peszynska, M., and Wheeler, M., 2003, Coupled fluid flow and geomechanical deformation modeling: Journal of Petroleum Science and Engineering, **38**, 37–56.

Nur, A., 1989, Four-dimensional seismology and (true) direct detection of hydrocarbons: the petrophysical basis: The Leading Edge, **8**, no. 9, 30–36.

Olden, P., Corbett, P., Westerman, R., Somerville, J., Smart, B., and Koutsabeloulis, N., 2001, Modeling combined fluid and stress change

effects in the seismic response of a producing hydrocarbon reservoir: The Leading Edge, **20**, 1154–1163.

Parashar, M., Pope, G., Wang, K., Wang, P., and Wheeler, J., 1997, A new generation EOS compositional reservoir simulator: Part II—Framework and multiprocessing: SPE Reservoir Simulation Symposium, Expanded Abstracts, 31–38.

Peaceman, D., 1977, Fundamentals of numerical reservoir simulation: Elsevier Scientific Publishing Company.

Pennington, W. D., Acevedo, H., Haataja, J., and Minaeva, A., 2001, Seismic time-lapse surprise at Teal South: That little neighbor reservoir is leaking!: The Leading Edge, **20**, 1172–1175.

Peszynska, M., Lu, Q., and Wheeler, M. F., 1999, Coupling different numerical algorithms for two phase fluid flow, *in* Whiteman, J. R., Ed., Proceedings of Mathematics of Finite Elements and Applications: Brunel University, 205–214.

Peszynska, M., Wheeler, M., and Yotov, I., 2002, Mortar upscaling for multiphase flow in porous media: Computational Geosciences, **6**, 73–100.

Rickett, J., and Lumley, D., 2001, Cross-equalization data processing for time-lapse seismic reservoir monitoring: A case study from the Gulf of Mexico: Geophysics, **66**, 1015–1025.

Sandler, I., and Rubin, D., 1979, An algorithm and a modular routine for the cap model: International Journal for Numerical and Analytical Methods in Geomechanics, **3**, 173–186.

Settari, A., and Mourits, F., 1994, Coupling of geomechanics and reservoir simulation models, *in* Siriwardane, and Zaman, Eds., Computer methods and advances in Geomechanics:: Balkema, 2151–2158.

Settari, A., and Walters, D., 1999, Advances in coupled geomechanical and reservoir modeling with applications to reservoir compaction: SPE Reservoir Simulation Symposium, Expanded Abstracts, 345–357.

Stone, C., 1997, SANTOS—A two-dimensional finite element program for the quasistatic, large deformation, inelastic response of solids: Sandia National Labs, Technical Report SAND90-0543.

Vidal, S., Huguet, F., and Mechler, P., 2002, Characterizing reservoir parameters by integrating seismic monitoring and geomechanics: The Leading Edge, **21**, 295–301.

Wang, P., Yotov, I., Wheeler, M., Arbogast, T., Dawson, C., Parashar, M., and Sepehrnoori, K., 1997, A new generation EOS compositional reservoir simulator: Part I—Formulation and discretization: SPE Reservoir Simulation Symposium, Expanded Abstracts, 55–64.

Wellman, G., 1999, MAPVAR—A computer program to transfer solution data between finite element meshes: Sandia National Labs, Technical Report SAND99-0466.

Wheeler, M., Arbogast, T., Bryant, S., Eaton, J., Lu, Q., Peszynska, M., and Yotov, I., 1999, A parallel multiblock/multidomain approach for reservoir simulation: SPE Reservoir Simulation Symposium, Expanded Abstracts, 51–61.

Wheeler, M. F., Wheeler, J. A., and Peszynska, M., 2000, A distributed computing portal for coupling multi-physics and multiple domains in porous media, *in* Bentley, L. R., Sykes, J. F., Brebbia, C. A., Gray, W. G., and Pinder, G. F., Eds., Computational methods in water resources:: A. A. Balkema, 167–174.

Xu, H., and Nur, A., 2001, Integrating reservoir engineering and satellite remote sensing for (true) continuous time-lapse reservoir monitoring: The Leading Edge, **20**, 1176–1179.

Yotov, I., 1998, Mortar mixed finite element methods on irregular multiblock domains *in* Wang, J., Allen, M. B., Chen, B., and Mathew, T., Eds., Iterative methods in scientific computation: International Association for Mathematics and Computers in Simulation, 239–244.